ELSEVIER

Contents lists available at ScienceDirect

Surface & Coatings Technology

journal homepage: www.elsevier.com/locate/surfcoat





Comparative tribological behavior of TiN monolayer and Ti/TiN multilayers on AZ31 magnesium alloys

Wenling Xie ^{a,c}, Yiman Zhao ^a, Bin Liao ^{b,*}, Shu Wang ^a, Sam Zhang ^{a,*}

- ^a Centre for Advanced Thin Films and Devices, School of Materials and Energy, Southwest University, Chongqing 400715, China
- ^b School of Nuclear Science and Technology, Beijing Normal University, Beijing 100875, China
- ^c School of Mechanical Engineering, Sichuan University of Science and Engineering, Zigong 643000, China

ARTICLE INFO

Keywords: Ti/TiN multilayer FCVA Wear resistance Magnesium alloy

ABSTRACT

The TiN monolayer and Ti/TiN multilayers were prepared on the AZ31 magnesium alloys by filter cathodic vacuum deposition. The TiN monolayer with highest hardness among the coatings failed during friction as its poor resistance to crack propagation, low toughness, and poor deformation coordination between the coating and substrate. The Ti/TiN multilayers with layered structure had lower hardness but withstood the friction process due to their higher toughness, better resistance to crack propagation and good deformation coordination between the coating and substrate. The layer by layer wear mechanism was revealed through observing the cross-sectional SEM morphology of the wear track of the Ti/TiN multi-2 coating. Compared with the Ti/TiN multi-2 coating, the Ti/TiN multil-6 coating with higher flow rate of nitrogen introduction had lower wear rate as its higher hardness but produced brittle cracks.

1. Introduction

Magnesium and magnesium alloys have attracted increasing interest due to their low density, high strength-to-weight ratio, thermal conductivity, biocompatibility [1], etc. They have a broad application in aerospace, military, electronics, sports, biomedical, and automobile industry [2,3] etc. Poor corrosion and wear resistance are the fatal defects hindering their wide application, and coating provides an economical and effective method to solve this problem [4–6]. Metal coating [7], hard ceramic coating with transition layer [8], composite coating [9], and multilayer coating [10] have good adhesion with magnesium alloy matrix, which can prevent the coating from failure in the process of corrosion and friction, thus have been widely used in corrosion or/and wear protection of magnesium alloys. Among them, composite and multilayer coatings can effectively improve wear resistance by reducing residual stress and increasing toughness without sacrifice of hardness. For example, Cr doped DLC coating [9], Al/AlN/CrAlN/CrN/MoS₂ gradient multilayer [10], and TiN/CrN alternate multilayers [11,12] reduced the wear rate of the magnesium alloys by nearly two orders of magnitude.

Titanium nitride (TiN) coating has high hardness and good wear resistance [13], and is widely used in tools and mechanical components,

but sudden brittle cracking or fatigue cracking are common in the working process [14]. Many studies have confirmed that appropriate matching of hardness and toughness, good fatigue resistance, and high coating/substrate bonding strength are the basis of excellent wear resistance of the coating [15,16]. So, the soft and plastic metallic Ti layer has been introduced to form Ti/TiN multilayer to achieve the following purposes: (1) improving toughness by preventing crack propagation in coating [17-20]; (2) reduce coating defects and density coating [20-22]; (3) improving adhesion strength by absorbing impact energy through the plastic deformation of Ti sublayer [23]. To date, Ti/TiN multilayers have been prepared on steels [24-27], iron [28], uranium [29], titanium alloys [30,31], epoxy based carbon fiber reinforced polymers [32] substrates for improvement of corrosion and wear resistance. After Ti/ TiN multilayer coating, the wear rate of sample is reduced by 1–2 orders of magnitude [24,26,29], and thicker Ti sublayer in Ti/TiN multilayer means better cracking resistance [31]. Thus, Ti/TiN multilayers is expected to improve wear resistance of magnesium alloy.

In this article, the TiN monolayer and Ti/TiN multilayers were prepared by filtered cathodic vacuum arc (FCVA) deposition on the AZ31 magnesium alloys. The mechanical property and wear resistance of the TiN monolayer and Ti/TiN multilayers with different coating structures were studied. By observing the cross-sectional SEM morphology of

E-mail addresses: liaobingz@bnu.edu.cn (B. Liao), samzhang@swu.edu.cn (S. Zhang).

^{*} Corresponding authors.

Table 1 Deposition parameters.

Parameters	TiN	Ti/TiN multi-2		Ti/TiN multi-6	
	monolayer	Ti	TiN	Ti	TiN
N ₂ flow rate (sccm)	2	0	2	0	6
Negative bias voltage (V)	100	100	100	100	100
Duty cycle (%)	50	50	50	50	50
Arc current (A)	90	90	90	90	90
Magnetic current (A)	2.0	2.0	2.0	2.0	2.0
Deposition time (min)	240	10	20	10	20
Alternation times	_	8	8	8	8
Pressure deposition	8.5×10^{-3}	7 ×	8.5 ×	7 ×	$1.0 \times$
(Pa)		10^{-3}	10^{-3}	10^{-3}	10^{-2}

coated silicon samples after friction for different times, the wear evolution and layer by layer wear mechanism of the Ti/TiN multilayer were revealed. Also, the effect of deformation of soft magnesium alloy substrate on the wear behavior of the TiN monolayer and Ti/TiN multilayers was studied.

2. Experimental

Square blocks of AZ31 magnesium alloy (mass fraction: 3.1~% Al, 0.9~% Zn, 0.32~% Mn, 0.012~% Si, 0.0089~% Cu, 0.0021~% Fe, 0.0009~% Ni, and Mg balance) with $20~\text{mm} \times 20~\text{mm} \times 2~\text{mm}$ size and silicon (100) wafers with 0.5~mm thickness were used as substrates. All AZ31 alloy samples were ground with 400–2000~grit SiC papers and then polished with alumina suspension with $1~\mu m$ particle size. After rinsed with deionized water, the polished AZ31 magnesium alloys and silicon species were ultrasonically cleaned in acetone and alcohol for 10~and~5~min,

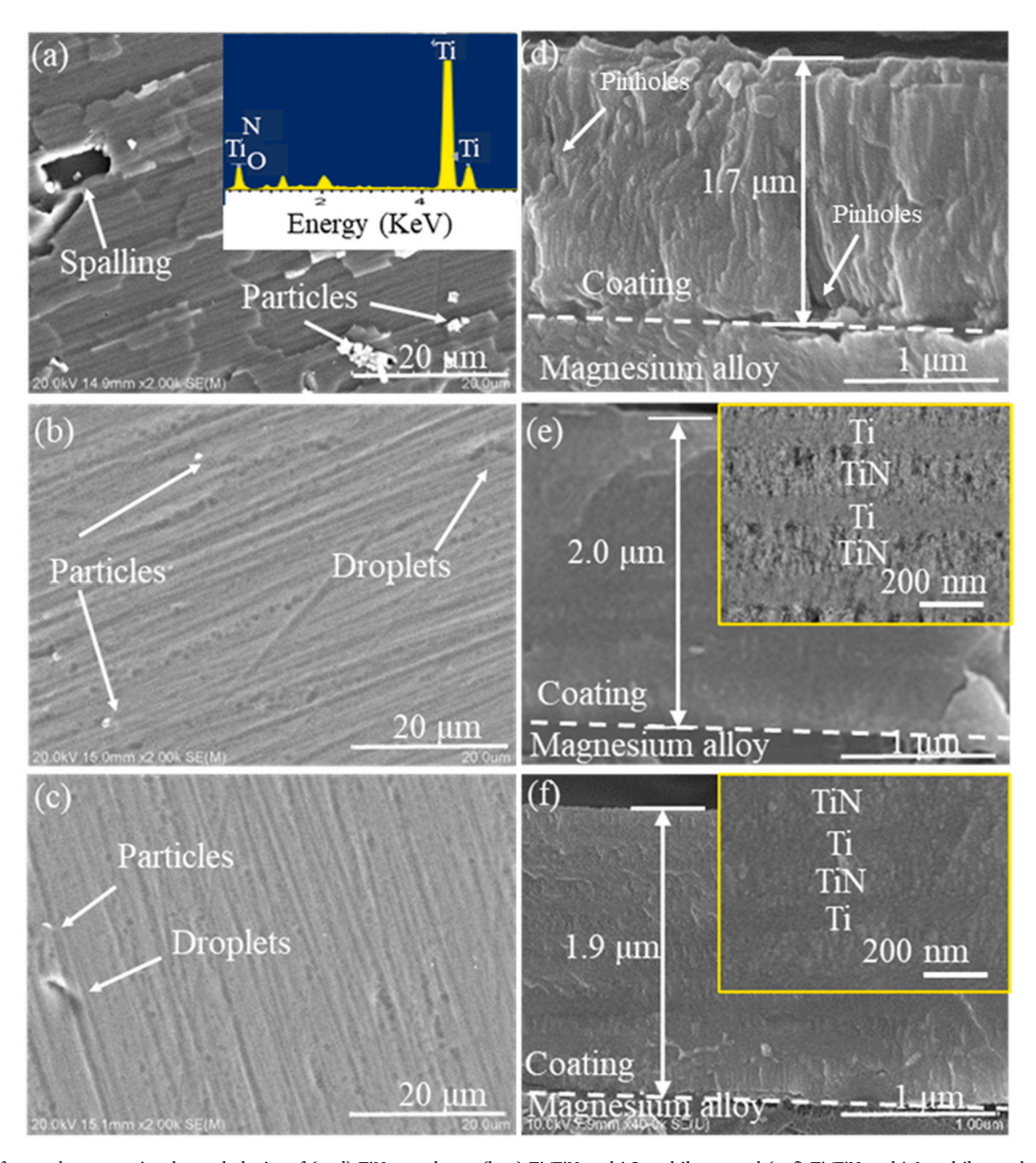


Fig. 1. Surface and cross-sectional morphologies of (a, d) TiN monolayer, (b, e) Ti/TiN multi-2 multilayer, and (c, f) Ti/TiN multi-6 multilayer, depicting local spalling and columnar crystal structure of the TiN monolayer and dense layered structure of the multilayers.

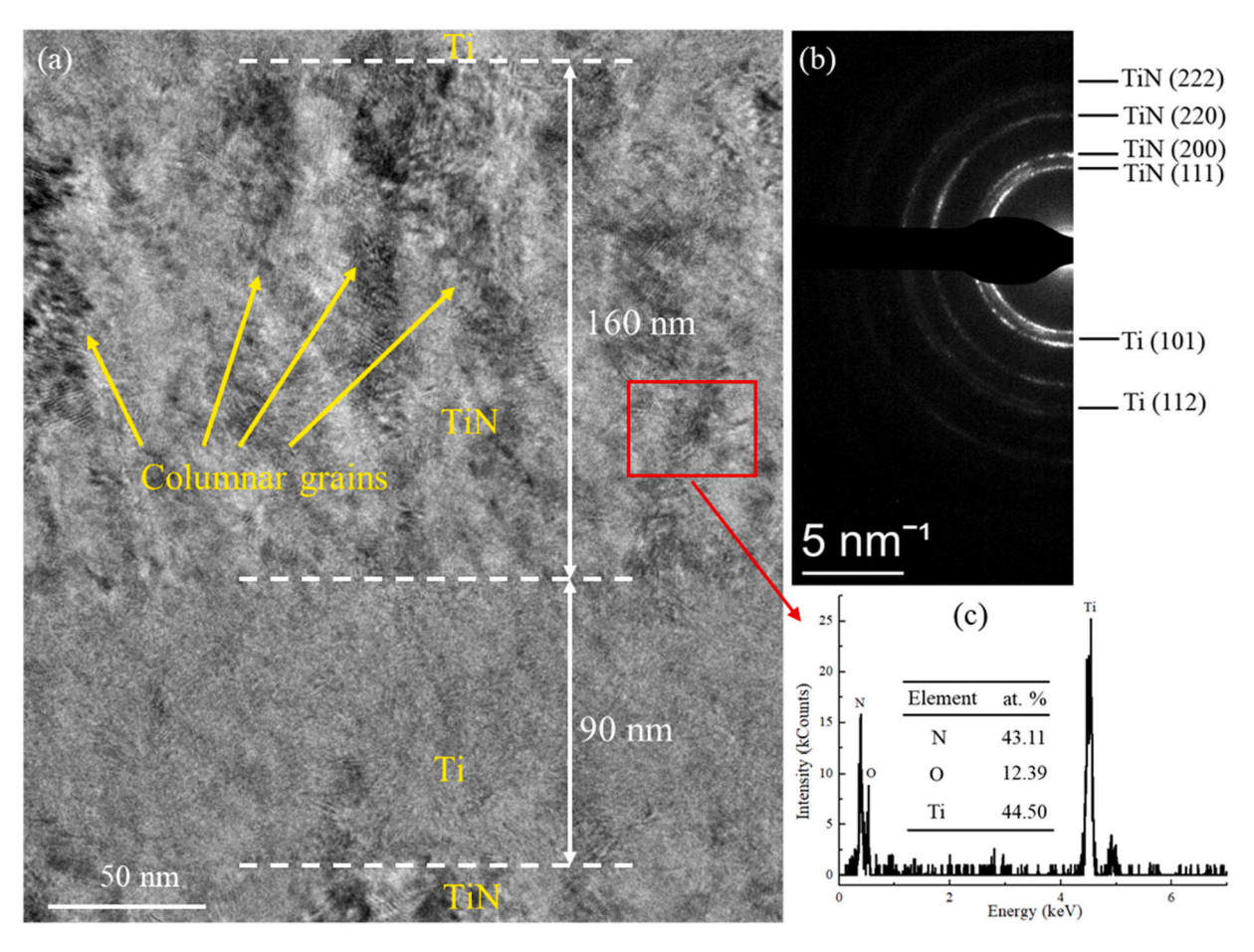


Fig. 2. (a) Bright field TEM image of the cross-sectional micrograph and (b) SAED pattern of the Ti/TiN multi-2 coating, and (c) EDS spectra of red rectangle in Fig. (a), depicting the layered structure of the Ti/TiN multi-2 coating, some columnar grains and near saturated N content in the TiN sublayer.

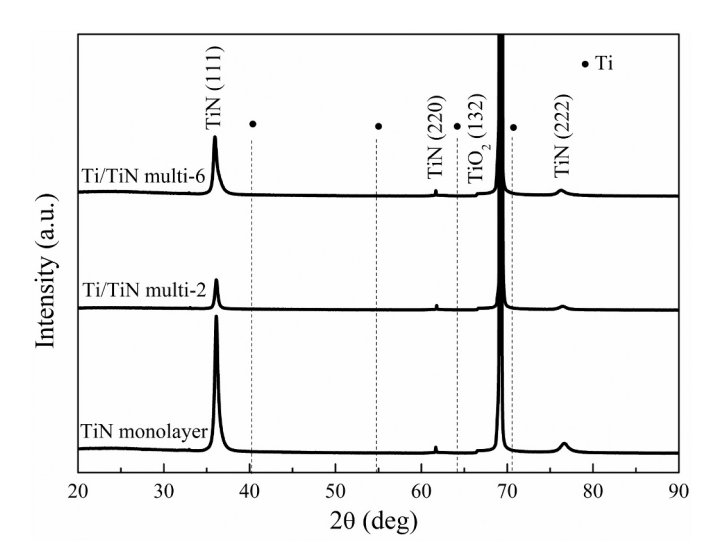
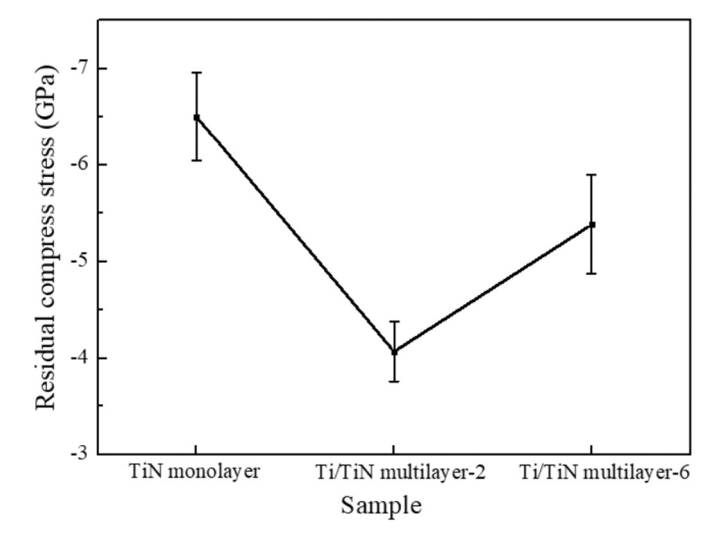


Fig. 3. XRD spectra of coatings on the Si substrates, all coatings show same peaks and preferential growth along the TiN (111) plane.

respectively, and followed by dried in cold air.

A filtered cathodic vacuum arc deposition system with a 180° magnetic filter elbow designed by Beijing Normal University was used to deposition of coating. The 180° magnetic filter elbow has a perfective filtering effect on large particles, effectively prevents the temperature rise during film deposition and obtains a denser coating. A titanium



 $\begin{tabular}{ll} Fig.~4. Residual compress stress of the TiN monolayer, Ti/TiN multi-2, and Ti/TiN multi-6 coatings, verifying the multilayers had lower residual stress. \\ \end{tabular}$

target (100 mm diameter) with 99.99 % purity was the cathode, 99.999 % purity nitrogen was used as the reaction gas. All samples were fixed on a rotatable sample holder keeping 20 cm from the outlet of the magnetic elbow. The chamber was firstly pumped to 4.0×10^{-3} Pa and then the samples were orderly sputter-cleaned at 600 and 400 V substrate negative biases for 30 s, respectively. After sputter-cleaning, all samples

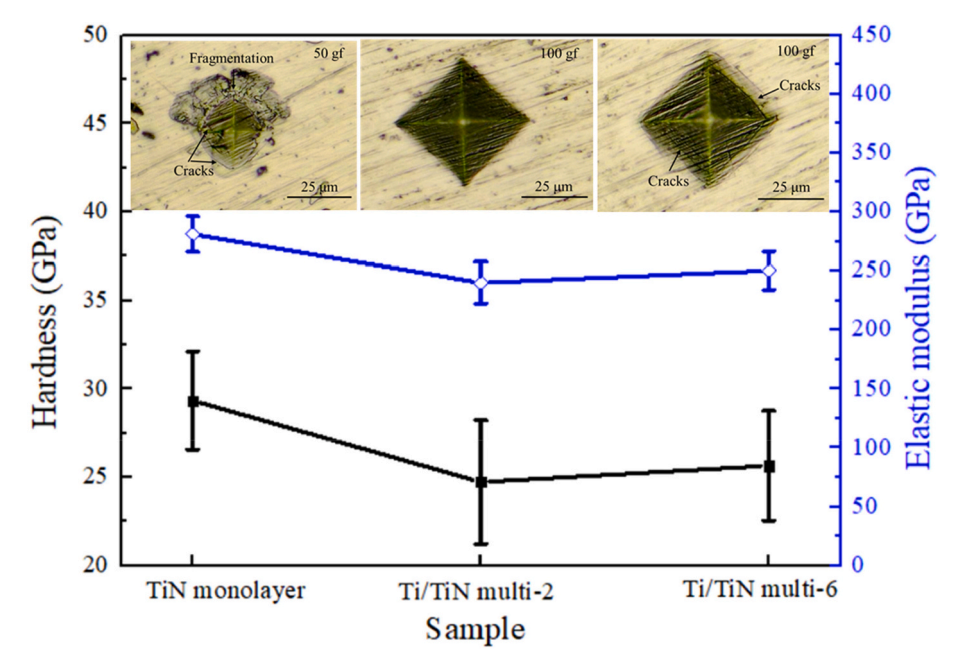


Fig. 5. Hardness and elastic modulus of nanoindentation, and the Vickers indentation images of the TiN monolayer and Ti/TiN multilayers under 50 and 100 gf loads, respectively. Which depicts the TiN monolayer has higher hardness, but lower toughness compared with the multilayers.

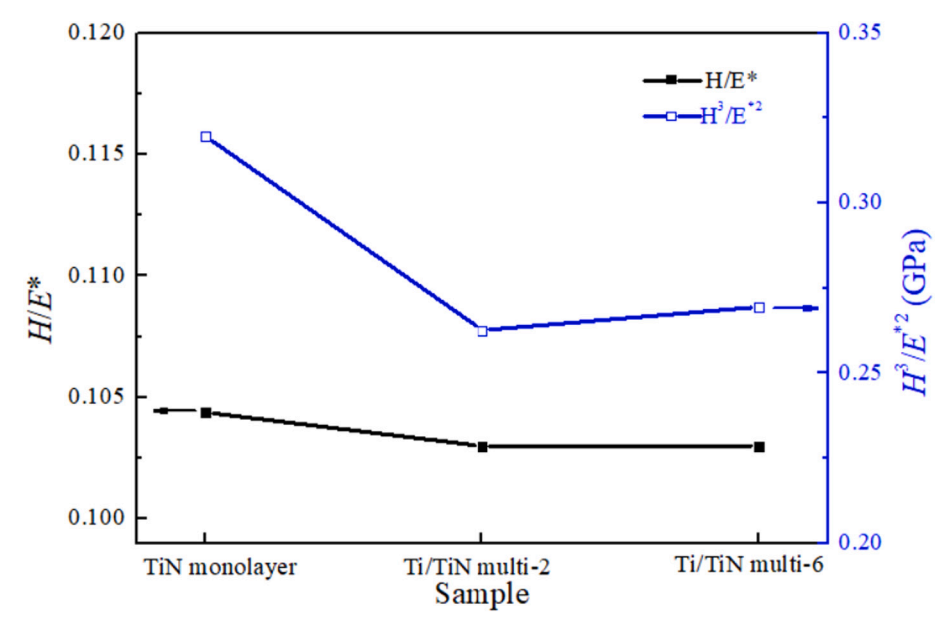


Fig. 6. Ratios of H/E^* and H^3/E^{*2} of the TiN monolayer and Ti/TiN multilayers, indicating the H/E^* and H^3/E^{*2} ratios of the coating from high to low is the TiN monolayer coating, Ti/TiN multi-6 coating, and Ti/TiN multi-2 coating.

had a suitable temperature and rough surface for good adhesion strength between the coating and substrate [33]. Both sputtering cleaning and coating deposition maintained 50 % duty cycle, 90 A arc current, and 2.0 A magnetic field. And 100 V substrate negative bias was used during coating deposition. A Ti transition layer was firstly deposited for 5 min to improve adhesion strength of coating, then 2 sccm flow rate of nitrogen was introduced for the TiN monolayer deposition. The Ti/TiN multilayers (named as Ti/TiN multi-2 and Ti/TiN multi-6) were deposited alternately for 10 min without $\rm N_2$ and 20 min with 2 and 6 sccm flow rate of $\rm N_2$ introduction, respectively. This process was repeated for 8 times. The total deposition time for all coatings was 240 min. The detailed parameters of the coating preparation are listed in Table 1.

The surface and cross-sectional morphologies of the coating on the

magnesium alloy substrate were observed by a field-emission scanning electron microscope (FESEM, Hitachi S-4800) equipped with EDS (Super-X EDS). The cross-sectional morphology of the Ti/TiN multi-2 coating was also observed by a field-emission transmission electron microscope (TEM, Thermo Fisher Talos F200) equipped with EDS (Super-X EDS) and was operated at 200 kV. the transmission sample were prepared by focused ion beam (FIB). The phases component of the coating was investigated by an X-ray diffraction (XRD, X pert pro MPD) with a Cu K α radiation ($\lambda=0.154056$ nm), operated at 40 kV and 40 mA.

A surface morphology examination (Talysurf 5P-120) was carried out for curvature of the Si sample before and after coating. Five measurements were executed and the average value was used to calculate the corresponding residual stress of the coatings using Stoney's equation

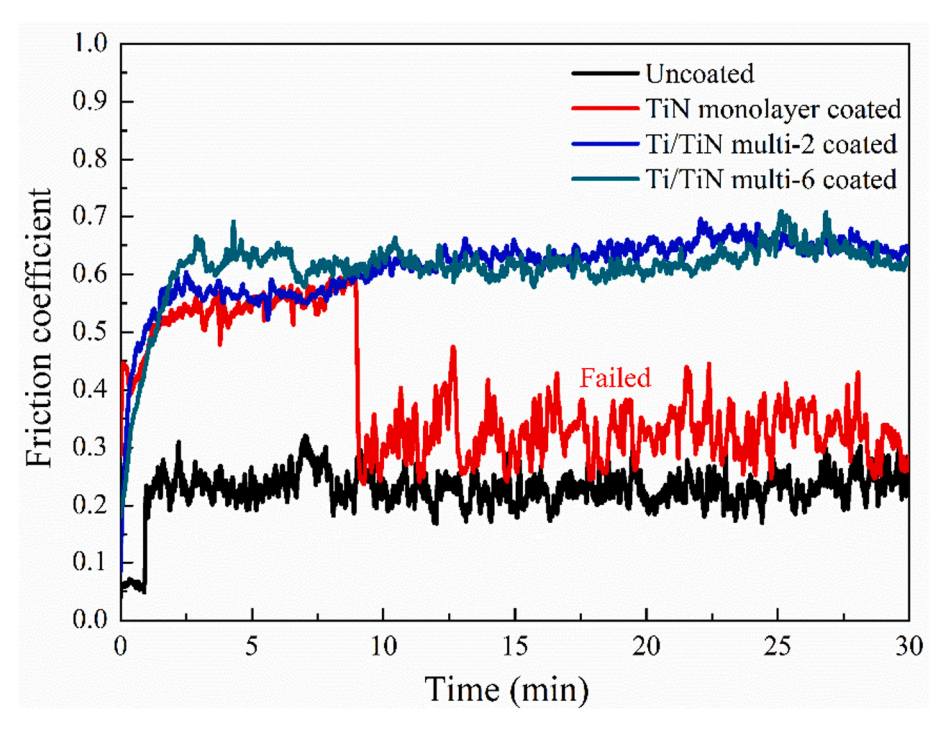


Fig. 7. Friction coefficient of the uncoated-, Ti/TiN multilayer-coated AZ31 magnesium alloys under 1 N load for 30 min. The TiN monolayer failed after friction for 9 min, and the Ti/TiN multilayers withstood whole friction process.

(Eq. (1)) [34]:

$$\sigma = \frac{1}{6} \frac{E_s t_s^2}{(1 - v_s)t_f} \left(\frac{1}{R_2} - \frac{1}{R_1} \right) \tag{1}$$

where E_s , v_s , and t_s are Young's modulus of (GPa), Poisson's ratio, and thickness (mm) of substrate, respectively. t_f is thickness (mm) of coating, R_2 and R_1 are curvature radius (mm) of substrate after and before coating.

An MMT-X7A Vickers hardness tester was used to evaluate the toughness of the TiN monolayer and Ti/TiN multilayers on the magnesium alloys at applied loads of 50 g and 100 g, respectively.

A nanoindenter G200 (Keysight Technologies) equipped with a Berkovich diamond probe tip was used to measure the hardness (H) and Young's modulus (E) of the coating. Compared with the conventional mechanical property testing technology, the surface state of the sample is more important to the test results of nano indentation method. The surface roughness of magnesium alloy substrate is larger than that of silicon substrate, thus the roughness of the coatings on magnesium alloys is correspondingly larger than that of coatings on silicon substrates. So, the nano indentation test was applied on the coated magnesium alloy. To minimize the effect of the substrate, the maximum loading force was 15 mN and the pressing depth was less than 200–230 nm (less than 1/8 of the coating thickness). Five measurements gave an average value for each sample.

The dry tribological performance of the uncoated- and coated magnesium alloys, and coated silicon wafers were tested using a reciprocating electrochemical corrosion friction and wear tester (MFT-EC4000). All tests were carried out in an ambient environment at room temperature against a $\rm Si_3N_4$ ball (6 mm diameter). A normal load of 1 N with the reciprocating friction distance of 5 mm and the frequency of 1 Hz were applied. For the coated magnesium alloys, the wear depth profile was gained by the surface morphology instrument (Talysurf 5P-120) after 30 min test. The wear rate was calculated from the following equation [35]:

$$W = V/(P \times L) \tag{2}$$

where W is wear rate (mm³/N. m), V is wear volume (mm³), L is sliding distance (m) and P is load (N). The wear track and elemental composition within wear track, the cross-sectional morphology and corresponding elemental mapping images of the coated magnesium alloys after friction were observed by SEM equipped with EDS. Also, the cross-sectional morphologies of the TiN monolayer coated Si sample for 10 min friction and Ti/TiN multi-2 coated Si sample for 5 to 120 min friction were observed by SEM.

3. Results and discussion

3.1. Microstructure

The surface and cross-sectional SEM morphologies of coatings on the magnesium alloys were shown in Fig. 1. Due to the magnetic elbow filtration of FCVA, only a few micro particles and droplets (Fig. 1 a-c) were observed on the surface of coatings [23,36]. The thickness of the TiN monolayer, Ti/TiN multi-2 coating, and Ti/TiN multi-6 coating was 1.7, 2.0, and 1.9 μm (Fig. 1 d-f), respectively. The TiN monolayer showed columnar structure with some detritus and local spalling on the surface, some visible pinholes were seen between columnar crystal boundary (Fig. 1 a, d). However, EDS result shows that there were Ti, N and O peaks in the spalling area and no magnesium peaks, indicating that the magnesium alloy was still completely covered by the coating. As shown in Fig. 1 e, f, the Ti/TiN multi-2 and Ti/TiN multi-6 coatings had clear layered structure because of alternate deposition of Ti and TiN layers, which can be explained by the crystal lattice mismatch between Ti and TiN [37]. There were no visible cracks and pinholes.

Fig. 2 shows bright-field TEM image of the cross-sectional micrograph and selected area electron diffraction (SAED) pattern of the Ti/TiN multi-2 film. For the Ti/TiN multilayer, some columnar grains (yellow arrows) in the TiN sublayer were interrupted by the Ti sublayer. Modulation TiN:Ti was \sim 1:1.8 (Fig. 2 a). The average thickness of the Ti and TiN sublayers was \sim 90 and \sim 160 nm for the Ti/TiN multi-2 coating, and \sim 85 and \sim 153 nm for the Ti/TiN multi-6 coating, respectively. Continuous polycrystalline diffraction rings were observed in Fig. 2b. Those rings were identified as the TiN (111), Ti (101), TiN (200), TiN

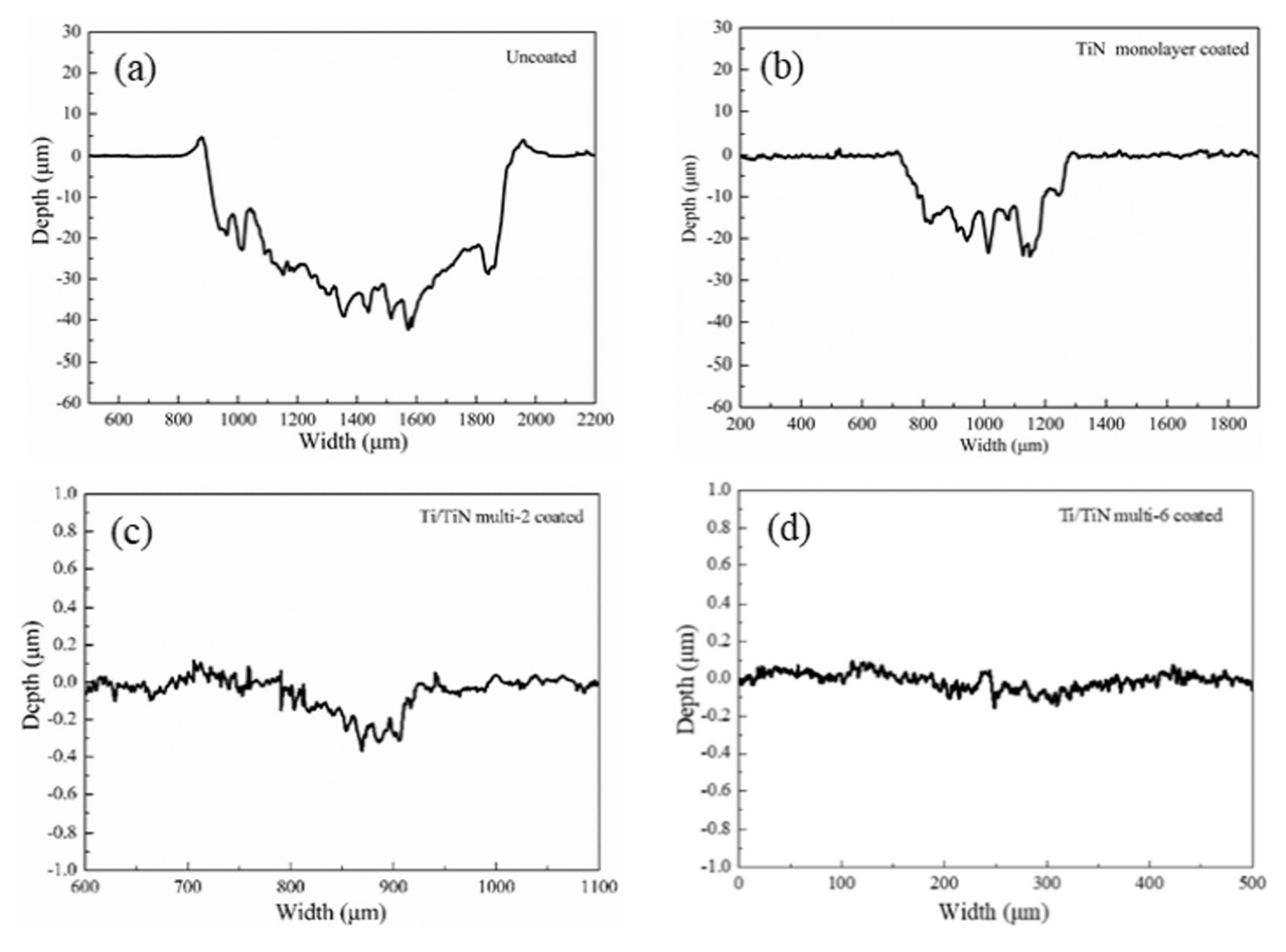


Fig. 8. The wear depth profile of the (a) uncoated-, (b) TiN monolayer coated-, (c) Ti/TiN multi-2 coated-, and (d) Ti/TiN multi-6 coated AZ31 magnesium alloys under 1 N load for 30 min. The wear depth of the TiN coating and Ti/TiN multilayers was higher and lower than thickness of the coatings, respectively, which means that the TiN monolayer failed during friction process and the Ti/TiN multilayers withstood friction process.

(220), Ti (112), and TiN (222) planes due to the d-spacings of 2.44, 2.26, 2.10, 1.48, 1.26, and 1.21 Å, respectively. Fig. 2c shows the content of elements of the red rectangle area in the TiN sublayer of the Ti/TiN multi-2 coating, the atom ratio of Ti/N/O was 44.50/43.11/12.39, inferring that nitrogen in the TiN sublayer of the Ti/TiN multilayer was almost saturated even if only 2 scm nitrogen was introduced. The O came from the residual air in the vacuum chamber [8]. Large area peeling of coating was found with a higher nitrogen flow rate of 8 sccm introduction, indicating that under the adopted parameters, 6 sccm is a critical value of nitrogen flow for the preparation of $\sim\!\!2~\mu m$ thick TiN coating and Ti/TiN multilayer on the AZ31 magnesium alloy.

3.2. Phases

All coatings had peaks of TiN (111), TiN (220), and TiN (222) at 36.1° , 61.8° , and 76.4° , respectively, as shown in Fig. 3, which are identified in the SAED pattern of the Ti/TiN multi-2 coating. No peak of Ti was found in the Ti/TiN multilayers, which may be due to the thin thickness or small grain size of the Ti sublayer. The TiO₂ (132) peak at 66.9° was related to reaction of the residual air and Ti plasma in the chamber during coating deposition [28,38], which is the reason for the existence of O element in the coatings (Table 1). All coatings showed preferential growth along the TiN (111) plane.

3.3. Mechanical properties

In the process of PVD, residual stress is always an inevitable

headache. Excessive residual stress will decrease adhesion of coating, resulting in early failure or spalling of coating in work [39,40]. All coatings had compressive residual stress due to ion bombardment during coating deposition. As shown in Fig. 4, the residual stress of the TiN coating was -6.5 ± 0.46 GPa. For the Ti/TiN multi-2 and Ti/TiN multi-6 coatings, the residual stresses were -4.07 ± 0.31 and -5.38 ± 0.51 GPa, respectively, 62.6 % and 82.8 % of that of the TiN monolayer. The multilayer structure significantly reduced the residual stress of coatings through elastic deformation of soft Ti sublayer [17,18,41], resulting in improvement of the bonding strength between the coating and substrate. Compared with the Ti/TiN multi-2 coating, higher residual stress of the Ti/TiN multi-6 coating was obtained due to stronger particle collision caused by more nitrogen introduction [42].

Fig. 5 shows the hardness (H) and elastic modulus (E) of coatings. H and E of the TiN monolayer, Ti/TiN multi-2 coating, and Ti/TiN multi-6 coating were 29.34 ± 2.77 GPa and 281.1 ± 15.20 GPa, 24.73 ± 3.50 GPa and 240.01 ± 17.57 GPa, and 25.65 ± 3.10 GPa and 250.25 ± 16.30 GPa, respectively. The Ti/TiN multilayers have lower hardness than the TiN monolayer have been reported in references [20,24,43], which is attributed to: (1) introduction of the softer plastic metal Ti sublayer [24,41,44] and (2) the lower residual stress of the Ti/TiN multilayers, since the decrease of compressive stress level in the coating is closely related to the decrease of hardness [14,45]. In addition, the residual stress increased due to higher ion bombardment energy, the hardness of the Ti/TiN multi-6 coating was slightly higher than that of the Ti/TiN multi-2 coating [46]. 50 gf and 100 gf applied loads were used to qualitatively test the indentation toughness of the TiN

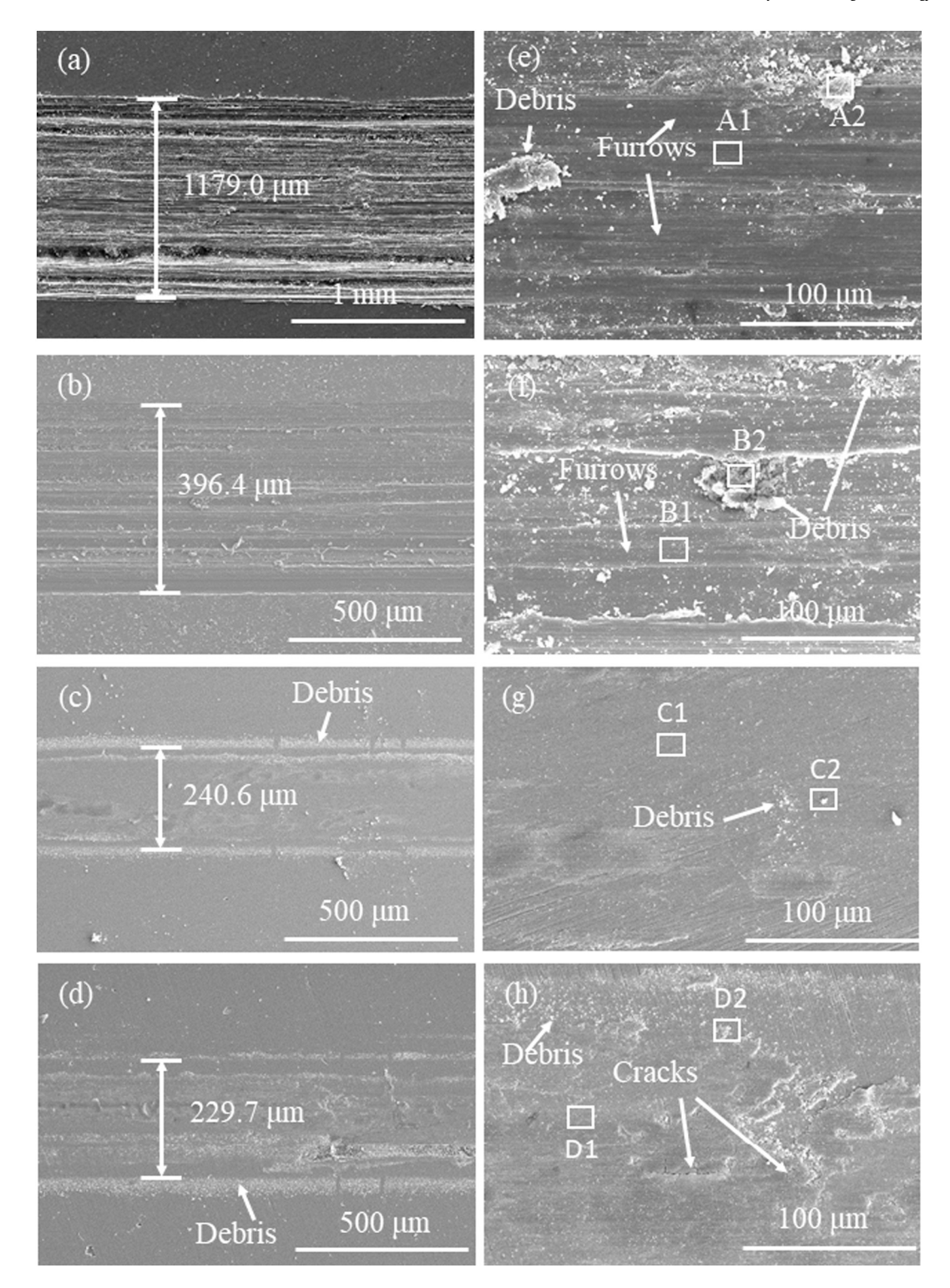


Fig. 9. SEM images of the wear scars of the uncoated- and coated AZ31 Mg alloys under 1 N load for 30 min at different magnification. (a, e) uncoated-, (b, f) TiN monolayer coated-, (c, g) Ti/TiN multi-2 coated-, and (d, h) Ti/TiN multi-6 coated samples, verifying the Ti/TiN multilayers' had excellent wear resistance.

monolayer coated- and Ti/TiN multilayer coated magnesium alloys, respectively. And the optical morphologies of Vickers indentation were inserted in Fig. 5. The TiN monolayer showed fragmentation and some cracks under 50 gf load. However, under 100 gf load, the Ti/TiN multi-2 coating showed no crack and the Ti/TiN multi-6 coatings showed a few annular cracks. The toughness of the coating from high to low is the Ti/TiN multi-2 coating, Ti/TiN multi-6 coating, and TiN monolayer coating. The toughness of the Ti/TiN multilayers is higher than that of

the TiN monolayer because the multilayers could dissipate energy through the plastic deformation of Ti sublayers [17,44,47], so the Ti/TiN multilayers had better resistance to crack propagation.

The H/E^* (elastic strain to failure) and H^3/E^{*2} (resistance to plastic deformation) ratios of coatings were shown in Fig. 6. The H/E^* ratios of the TiN monolayer, Ti/TiN multi-2 coating, and Ti/TiN multi-6 coating were 0.104, 0.103, and 0.103, respectively. The TiN monolayer had slightly higher H/E^* ratio than the Ti/TiN multilayers. The H^3/E^{*2} ratios

Table. 2 Elemental contents within the wear track of the uncoated- and coated AZ31 Mg alloys from Fig. 9.

Sample	Area	Element (at. %)							
		N	О	Mg	Al	Si	Ti		
AZ31 substrate	A1	0.00	1.61	94.92	3.43	0.04	_		
	A2	0.00	23.86	72.98	2.83	0.33	_		
TiN monolayer	B1	0.00	19.59	77.80	2.40	0.03	0.18		
Ti/TiN multi-2	B2	0.00	61.38	36.60	1.80	0.12	0.10		
	C1	19.13	17.56	_	_	0.07	63.23		
	C2	10.20	56.52	_	_	0.72	32.56		
Ti/TiN multi-6	D1	21.69	15.68	-	-	0.05	62.58		
	D2	7.03	59.47	-	-	1.22	32.28		

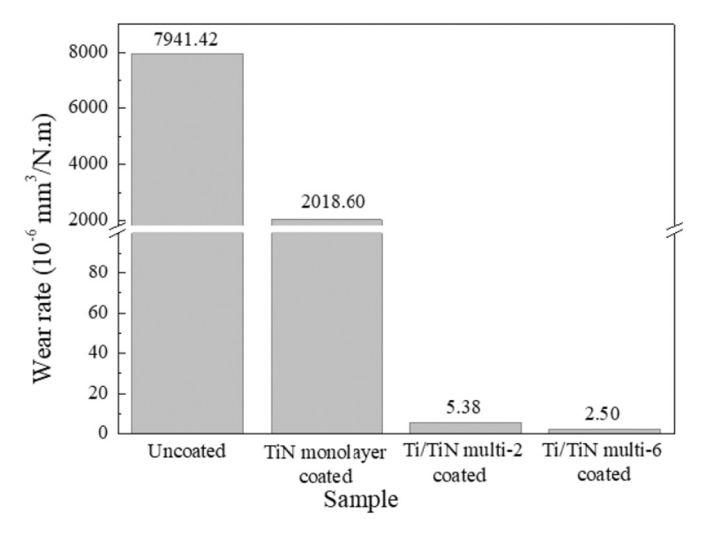


Fig. 10. Wear rate of the uncoated- and coated AZ31 magnesium alloys under 1 N load for 30 min, depicting the wear rate of the Ti/TiN multilayers is more than 3 orders of magnitude lower than that of the substrate.

of the TiN monolayer, Ti/TiN multi-2 coating, and Ti/TiN multi-6 coating were 0.320, 0.262, and 0.269 GPa, respectively. From high to low, the H^3/E^{*2} ratios is the TiN monolayer coating, Ti/TiN multi-6 coating, and Ti/TiN multi-2 coating.

3.4. Wear and friction performance of coatings

Fig. 7 shows the coefficient of friction (COF) during 30 min dry sliding performed on the uncoated- and coated magnesium alloys. For the uncoated AZ31 magnesium alloy, an average friction coefficient value of 0.23 was gained. The TiN monolayer and Ti/TiN multilayers led to higher COF, consistent with previous findings by other researchers [9,48]. For the TiN monolayer coated sample, COF firstly rose to 0.52 in the first 1 min and then gradually increased to 0.6. After 9 min friction, it abruptly declined to 0.25 (close to that of the uncoated sample) and oscillated strongly in the range of 0.25-0.45. The sudden drop in COF indicates the failure of the TiN monolayer. The strong oscillation of COF is attributed to two aspects: (1) the contact between the grinding ball and magnesium alloy with lubricating effect led to the reduction of COF and (2) some hard peeled particles remained in the wear mark and moved with the grinding ball, which led to the increase of COF. Furthermore, when hard Si₃N₄ ball cuts into the wear surfaces of the coatings under the normal load at the beginning of wear, the higher hardness and elastic modulus of the coating means the lower cut in depth of the Si₃N₄ ball. Additionally, the Si₃N₄ ball is mainly load on the micro-protrusions of wear surfaces of the coatings at the beginning of friction. The higher the hardness of the coating, the easier the micro convex surface is to be damaged under the action of tangential force. The combination of the above factors makes the TiN monolayer with higher hardness and elastic modulus has lower but faster increasing friction coefficient in the first 1-9 min.

In the case of the Ti/TiN multi-2 coated- and Ti/TiN multi-6 coated specimen, the friction coefficient value instantly rose to 0.58–0.65 and 0.62–0.65 in 7 min, respectively, then kept a relatively stable friction coefficient values of around 0.62 and 0.6 until the end of friction, respectively. Both the Ti/TiN multi-2 coated- and Ti/TiN multi-6 coated specimen withstood the friction process.

The wear depth of the uncoated- and coated AZ31 magnesium alloys under 1 N load after friction for 30 min was shown in Fig. 8. And the SEM images of wear scar at different magnification and the EDS results of the elemental contents within wear scar were shown in Fig. 9 and Table. 2, respectively.

The wear depth of the uncoated sample excessed 40 μ m (Fig. 8 a) and the wear width was 1179.0 μ m (Fig. 9 a). Deep furrows and a great deal of debris were observed in Fig. 9 a, e. EDS result shows that the oxygen content in furrows (A1) was low and that in debris (A2) was high, which means these debris was seriously oxidized to form MgO during friction process.

Compared with the uncoated sample, the TiN monolayer coated

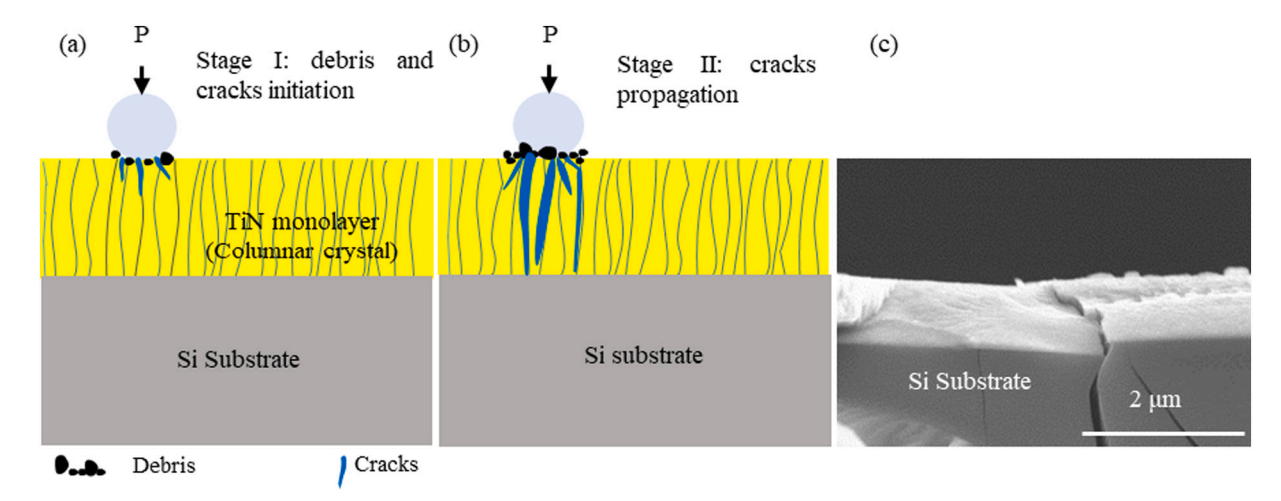


Fig. 11. The model of crack development in the TiN monolayer during friction procedure (a-b). (a) stage I: debris and cracks initiation, (b) stage II: crack propagation along the columnar crystal, and (c) cross-sectional SEM image of the TiN monolayer on the Si substrate after friction for 10 min, verifying the poor resistance to crack propagation and the failure of the TiN monolayer.

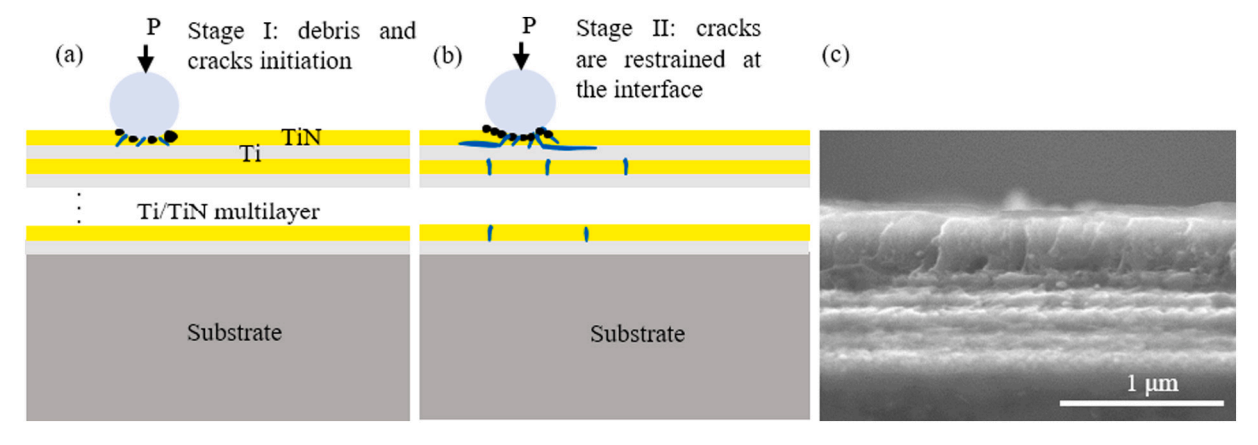


Fig. 12. The model of crack development in Ti/TiN multilayer during friction procedure (a-b). (a) stage I: debris and cracks initiation, (b) stage II: cracks are restrained at the interface, depicting crack propagation was hindered by the layered structure of the Ti/TiN multilayer, and (c) cross-sectional SEM image of the Ti/TiN multi-2 on the Si substrate after friction for 10 min under 1 N, verifying excellent resistance to crack propagation of the Ti/TiN multilayer.

sample showed shallower furrows and a lot of debris (Fig. 8 b, f). The wear width and wear depth were decreased to 396.4 μ m (Fig. 9 b) and below 25 μ m (Fig. 8 b), respectively. The wear depth was still much larger than the coating thickness, inferring that the TiN monolayer was completely worn after a period of friction, which is why the friction coefficient suddenly dropped to 0.25–0.45 after friction for 9 min (Fig. 7). The failure of the TiN monolayer was also confirmed by the high Mg content of furrow (B1, 77.8 %) and debris (B2, 33.6 %), as the Mg element came from the substrate. Furrows and debris were also seen in Fig. 9 b, f. Furrows (B1) and debris (B2) both had higher oxygen content as oxidation wear. The hard TiN monolayer could not provide long-term friction protection for the magnesium alloy.

Both the Ti/TiN multilayers coated AZ31 Mg alloys showed much shallower and narrower wear scars, fewer debris, and no furrow comparing to the uncoated- and TiN coated samples, as shown in Fig. 8 c, d and Fig. 9 c, d. Debris were accumulated on the outside of the wear tracks. For the Ti/TiN multi-2 and Ti/TiN multi-6 coatings, the wear width was 240.6 and 229.7 $\mu m,$ and the wear depth was less than 0.4 and $0.2~\mu m$, respectively. Both the Ti/TiN multilayers withstood friction procedure due to the wear depth is less than coatings thickness. That is the reason for they showed stable coefficient of friction. High Ti and N contents, and no Mg and Al contents were detected within wear scars of the Ti/TiN multilayers (C1, C2, D1, and D2) infers that the Ti/TiN multilayers kept integrity after whole friction procedure. High O contents of the debris (C2 and D2) of the Ti/TiN multi-2 and Ti/TiN multi-6 coatings indicates that oxidation occurred and TiO2 was formed during friction process [29]. Furthermore, compared with the Ti/TiN multi-2 coating, the Ti/TiN multi-6 coating showed some cracks within the wear scar, this can be explained by its higher hardness and lower

The wear rate of the uncoated-, TiN coated-, Ti/TiN multi-2 coated-, and Ti/TiN multi-6 coated AZ31 magnesium alloys under 1 N load for 30 min was 7941.42 \times 10 $^{-6}$, 2018.60 \times 10 $^{-6}$, 5.38 \times 10 $^{-6}$, and 2.50 \times 10 $^{-6}$ mm 3 /N. m, respectively, as shown in Fig. 10. Compared with the Ti/TiN multi-2 and Ti/TiN multi-6 coatings, although the TiN monolayer had higher hardness, higher wear rate was obtained due to its failure after friction for 9 min. The wear rates of the multilayers are three orders of magnitude lower than that of the uncoated sample. The Ti/TiN multilayers provided marvelous friction protection for the magnesium alloys. Owning similar layered structure and equal H/E^{\ast} ratio, the Ti/TiN multi-6 coating had lower wear rate than the Ti/TiN multi-2 coating due to its higher hardness and $H^3/E^{\ast 2}$ ratio [49].

The significant difference in wear rate between the TiN monolayer and Ti/TiN multilayers infers that the coatings with different structures have different wear behaviors and mechanisms [50]. In addition, for the soft magnesium alloy substrate, its deformation during friction

procedure may affect the friction and wear behavior of coating, which needs to be clarified.

3.5. Wear behaviors and mechanisms of the TiN monolayer and Ti/TiN multilayer during friction

So far, the effects of Ti/TiN multilayers with different modulation ratios [17,26], periods [41,51,52], sublayers number, and integrity thickness [32] on the improvement of mechanical property, corrosion resistance, and wear resistance were widely studied. Some papers have studied the deformation mechanism of multilayers under static load. For example, W. Yang et al. [53] studied the deformation mechanisms in Ti/ TiN multilayer under compressive loading by molecular dynamic simulations combined with atomically informed Frank-Bilby method. Ł. Majoret et al. [54] found that the vertical cracks of Ti/TiN multilayer only existed in the TiN sublayer using transmission electron microscope (TEM). They regard that it will result in layer-by-layer wear of the Ti/ TiN multilayer coating. However, they did not discuss this phenomenon in detail. Under nano indentation, J. Lackner et al. [16] found that the brittle cracks of the TiN monolayer propagated towards the surface along the columnar grain boundaries, while propagation of microcracks in the Ti/TiN multilayer along columnar crystals of the TiN sublayer stopped at the Ti/TiN interface. The layer by layer wear mechanism of the Ti/TiN multilayer was revealed by observation of cross-sectional TEM morphology after friction.

3.5.1. Establishment of crack propagation models of the TiN monolayer and Ti/TiN multilayer under friction load

To reveal the wear mechanisms of the TiN monolayer and Ti/TiN multilayer (Ti/TiN multi-2), two models of crack initiation and propagation during friction process were established and verified in Figs. 11 and 12, which consists of two stages. The hard silicon wafers were used as the substrates to eliminate the influence of plastic deformation of the soft magnesium alloy substrate on the wear behavior of coating. The stage I of both coatings is the same, that is, crack initiation and debris formation, as shown in Fig. 11 a and Fig. 12 a, and with the increase of friction time, debris and cracks increase, and stress is concentrated at the crack tip.

The stage II of the two coatings is significantly different. For the TiN monolayer, when the stress accumulates to a certain extent, the crack propagates along the columnar crystal of the coating due to the poor adhesion between columnar crystals in the hard brittle TiN monolayer [20], as shown in Fig. 11 b. Therefore, the crack rapidly penetrates through the coating thickness, leading to the coating collapses and failed. It was confirmed by the cross-sectional SEM image of the TiN monolayer after friction for 10 min (Fig. 11 c). For the Ti/TiN multi-2

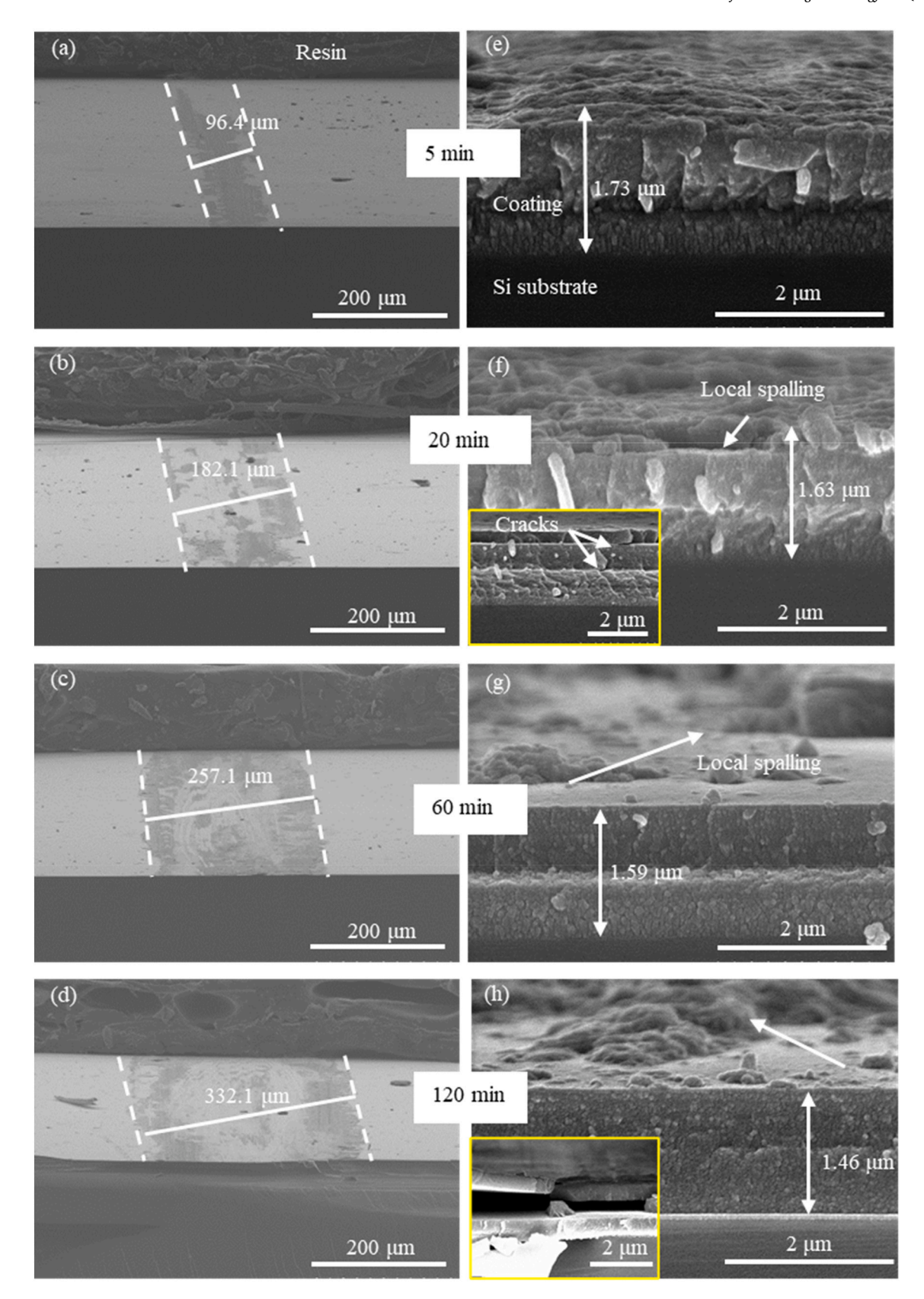


Fig. 13. Surface and cross-sectional morphologies of the Ti/TiN multi-2 coating after friction for different times. With increase of friction time, the Ti/TiN multilayer was worn layer by layer.

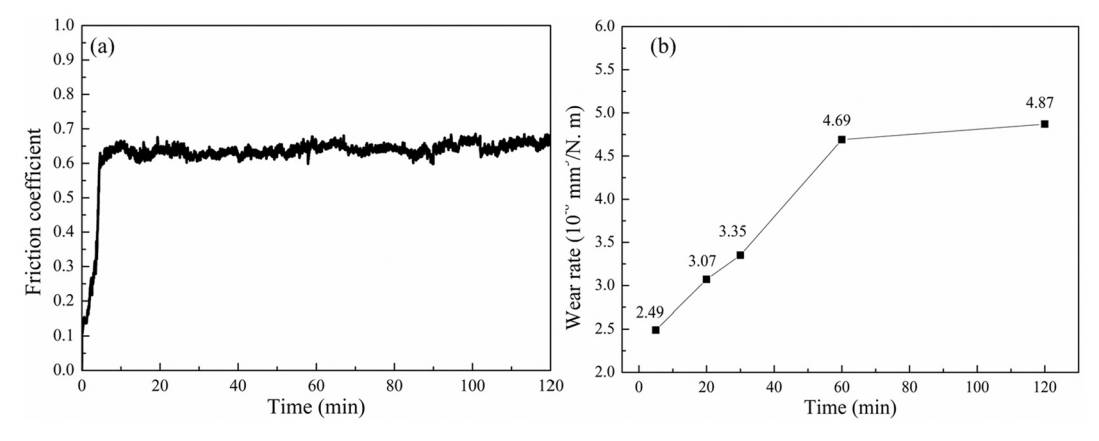


Fig. 14. (a) Friction coefficient during 120 min of the Ti/TiN multil-2 coated Si wafer under 1 N load and (b) corresponding wear rate after friction for 5 to 120 min, describing the Ti/TiN multilayer had good wear resistance and low wear rate.

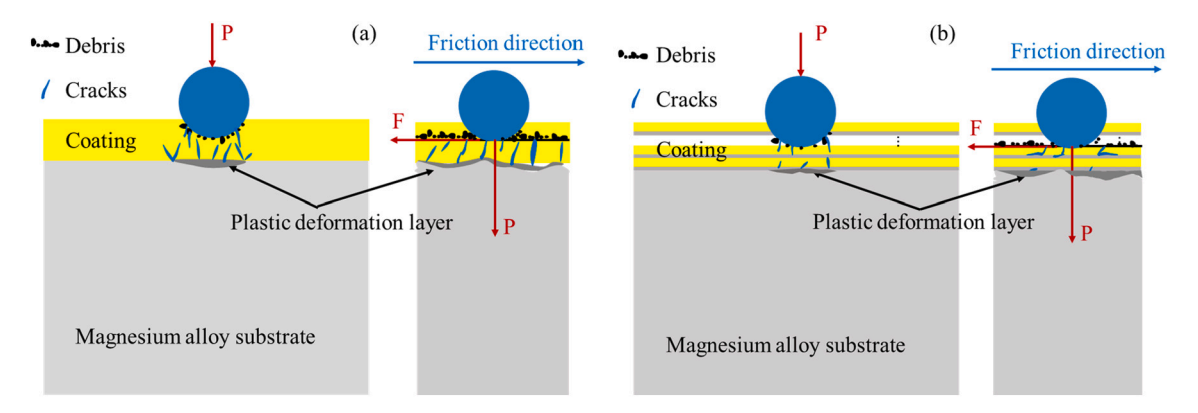


Fig. 15. Schematic diagram of stress and deformation of (a) TiN monolayer coated- and (b) Ti/TiN multilayer coated samples during friction procedure, describing the formation of debris and cracks of the coating, and the plastic deformation layer of the magnesium alloy substrate.

coating, the crack propagation is restrained at the Ti/TiN interface, as shown in Fig. 12 b. This is due to these aspects: (1) good plasticity and toughness of the soft Ti sublayers can restrain crack propagation. Some authors have observed the cracks produced in the TiN sublayer are deflected [55] or were stopped at the TiN/Ti interfaces [16,31,54]; (2) after the strain hardening of Ti sublayer, the deformation is transferred from Ti sublayer to TiN sublayer. Ti and TiN layers co-deform to avoid crack initiation [53]; (3) higher toughness of the multilayer can reduce the brittleness of coating and inhibit crack propagation [20,56]. Therefore, the Ti/TiN multi-2 coating exhibited no cracks and the coating did not fail after friction for 10 min under 1 N, as shown in Fig. 12 c.

3.5.2. Wear evolution of the Ti/TiN multilayer

The wear evolution of the Ti/TiN multilayer was studied by analyzing the cross-sectional SEM morphology of the coated Si sample after friction for 5 to 120 min under 1 N load, respectively, as shown in Fig. 13. The wear width of the coating after friction for 5, 20, 60, and 120 min was 96.4, 182.1, 257.1, and 332.1 μm , respectively, as shown in Fig. 13 a-d. The wear depth of the coating was 1.73, 1.63, 1.59, and 1.46 μm , respectively, as shown in Fig. 13 e-h. After friction for 5 min, as shown in Fig. 13 e, the coating surface became rough after slight wear. After friction for 20 min (Fig. 13 f), the outer sublayer of the coating was obviously worn, and the smooth Ti/TiN sublayer interface was observed locally. Some cracks along the Ti/TiN interface indicates that the wear developed along the Ti/TiN interface. After friction for 60 min, wear was more severe (Fig. 13 g). The wear extended along parallel direction of the Ti/TiN interface (the white arrow), the wear area of the coating was enlarged, some debris were remained within the wear area. After

friction for 120 min (Fig. 13 h), coating was stripped along the Ti/TiN interface (inserted image). However, the remained sublayers of the Ti/TiN multilayer were still closely bonded to the magnesium alloy substrate. To sum up, the coating was worn layer by layer with increase of friction time.

Fig. 14 shows COF during 120 min dry sliding performed on the Ti/ TiN multi-2 coated Si wafer under 1 N load and the corresponding wear rate after friction for different times. As shown in Fig. 14 a, the friction coefficient value rose to 0.62-0.65 in 6 min and then kept stable until the end of friction. That is, the COF value of the coating on the Si wafer is close to that of on the magnesium alloy. After friction for 5, 20, 30, 60, and 120 min, the wear rate of the Ti/TiN multi-2 coating was 2.49 \times 10^{-6} , 3.07×10^{-6} , 3.35×10^{-6} , 4.69×10^{-6} , and 4.87×10^{-6} mm³/N. m, respectively, as shown in Fig. 14 b. With the increase of wear time, the wear rate increased, however, the increase amplitude decreased, which means that the multilayer film had a relatively stable wear rate after wear for a period of time. This phenomenon should be attributed to the good matching of hardness and toughness of the multilayer film. Furthermore, the wear rate of the Ti/TiN multi-2 coating on the Si wafer was slighter lower than that on the magnesium alloy $(5.38 \times 10^{-6} \text{ mm}^3 /$ N. m) after friction for 30 min, this may be due to the local overall collapse of the magnesium alloy substrate resulted in concave and convex of the coating and intensified wear of the coating surface.

3.5.3. Wear behavior of the Ti/TiN multilayer on the magnesium alloy substrate

The hardness of the magnesium alloy is much lower than that of the Si plate. Under friction load, the magnesium alloy will deform. Fig. 15 shows the stress and deformation of the TiN monolayer coated- and Ti/

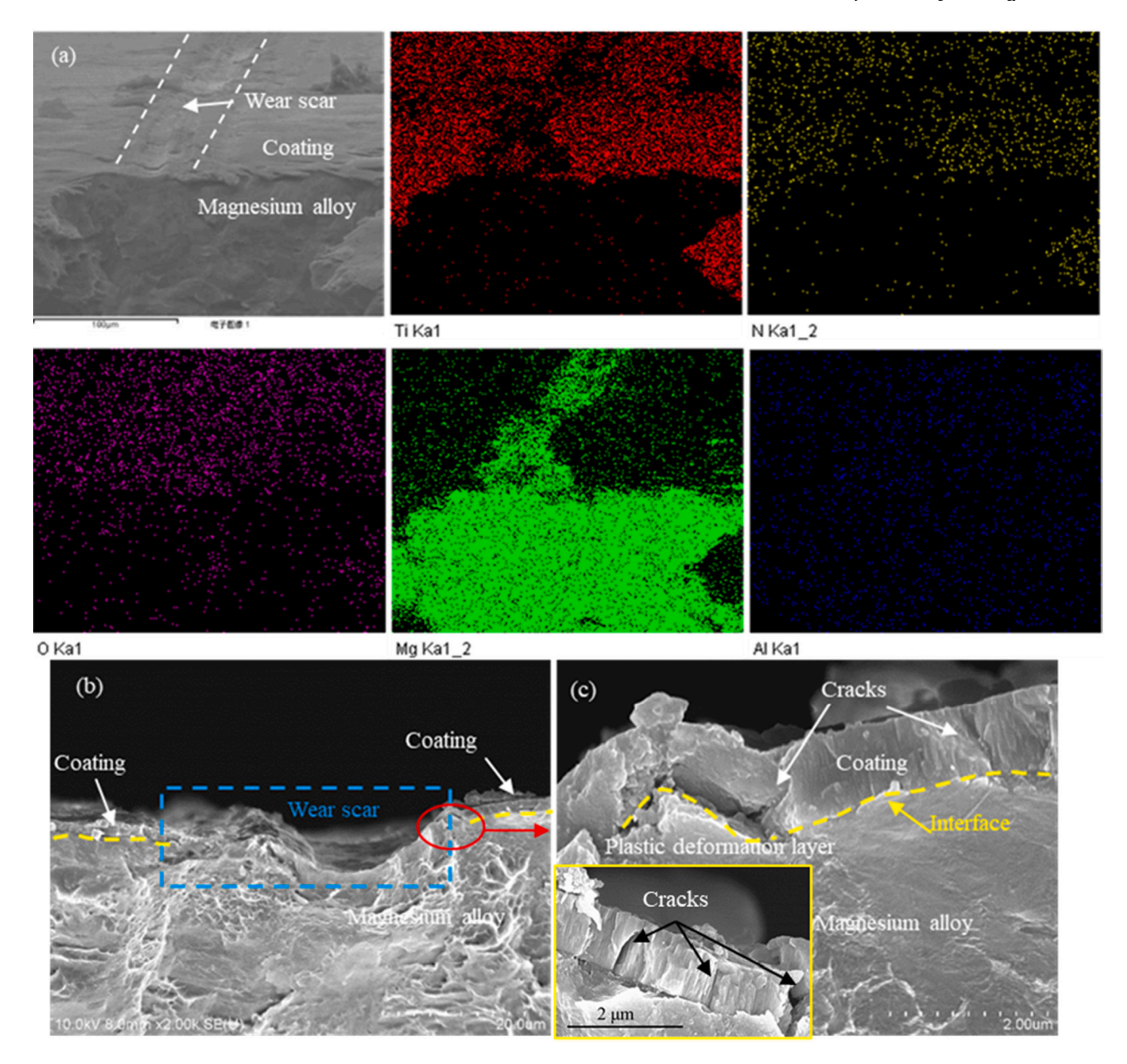


Fig. 16. (a) surface morphology and elemental mapping images, (b) cross-sectional morphology, and (c) enlarged images of the red ellipse in (b) of wear mark of the TiN monolayer on the magnesium alloy after friction for 10 min. The TiN monolayer failed and peeled off.

TiN multilayer coated AZ31 magnesium alloys during friction. Under friction load (P), the grinding ball relatively moves on coating, frictional force F is generated along the opposite direction of movement. With friction time increasing, debris and cracks are formed, coating produces elastic and plastic deformation. Subsequently, the soft magnesium alloy matrix deforms caused by stress transmitted through the coating, and the plastic deformation layer is formed. Then, the coating combined with the magnesium alloy substrate deforms harmoniously.

There is a great difference in plasticity between the soft magnesium alloy and hard brittle TiN monolayer, after the substrate deforming, the coordinated deformation ability of the TiN coating is poor. The coating adjacent to the coating/substrate interface cracks under stress. Then, the crack extends along the thickness of the coating and meets the crack formed during friction to form through-thickness crack. At the same time, the deformation of the substrate and the coating is different, leading to deterioration of coating adhesion. As a result, and the TiN coating locally loses the support of the substrate and peels off [57]. Fig. 16 shows the surface and cross-sectional SEM morphologies and

corresponding elemental mapping images of wear mark of the TiN monolayer after 10 min of friction under 1 N load and 1 Hz frequency. The wear depth was much deeper than coating thickness, as shown in Fig. 16 b (blue dashed rectangle), and the absence of Ti and N elements and the appearance of Mg element means the TiN coating was completely worn out. There is little difference in oxygen content between inside and outside the wear mark, indicating that the oxidation of the coating was slight during friction. The collapse and plastic deformation layer of the magnesium alloy matrix and through-coating cracks were seen, the coating collapsed and peeled off from the matrix, as shown in Fig. 16 c (enlarged image of the red oval in Fig. 16 b), which is consistent with the model in Fig. 15 a.

Fig. 17 shows surface and cross-sectional SEM morphologies and corresponding elemental mapping images of the Ti/TiN multi-2 coating on the magnesium alloy after friction for 30 min under 1 N load and 1 Hz frequency. After friction, in Fig. 17 a, the coated magnesium alloy was still covered by the coating, which is confirmed by the uniformly distribution of Ti and N elements and the absence of Mg element within the

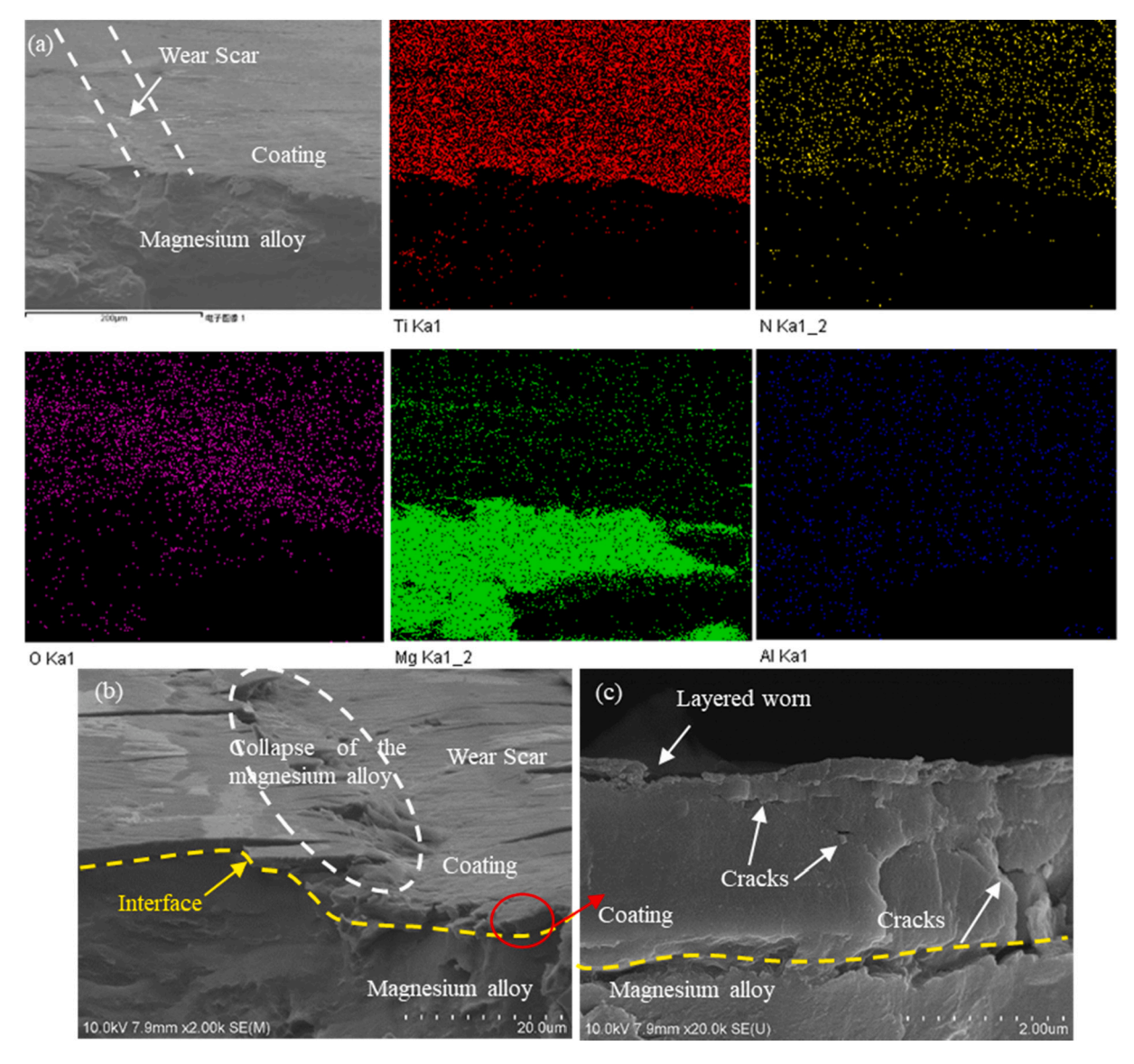


Fig. 17. (a) surface morphology and element distribution, (b) cross-sectional morphology, and (c) enlarged cross-sectional morphology of wear mark of the Ti/TiN multi-2 coating on the magnesium alloy after friction for 30 min, describing the layer by layer wear mechanism of the multilayer.

wear track. As same as the TiN monolayer, slight oxidation occurred during friction. The magnesium alloy matrix near the boundary of the wear scar seriously deformed and collapsed, as shown in Fig. 17 b (white dashed ellipse). However, the Ti/TiN multilayer had good coordinated deformation with magnesium alloy substrate, which is attributes to two aspects: (1) the "soft" Ti metal layers act as shear bands, allowing hard TiN layers to slide with each other to gain high deformation ability [25]; (2) multiple interfaces can dissipate energy, deflect cracks, and hinder crack propagation (Fig. 15 b) [58]. Therefore, there was no crack at the coating/substrate interface, the Ti/TiN multilayer was still combined with the magnesium alloy substrate and obtain the support of the substrate, as shown in Fig. 17 c. Some discontinuous cracks were seen along the parallel direction of the Ti/TiN interface, indicating that the cracks were deflected at the interface. The delamination of the outer sublayer of the coating (Fig. 17 c) during friction proved the layer by layer wear mechanism of the Ti/TiN multilayer.

4. Conclusions

The TiN monolayer and Ti/TiN multilayers were prepared on the AZ31 magnesium alloys by filter cathodic vacuum arc deposition. Wear

resistance of the coatings and wear mechanisms depending on coating structures were investigated, and the following conclusions were drawn:

- (1) The TiN monolayer has columnar crystal structure, while the Ti/TiN multilayers shows dense layered structure. Compared with the TiN monolayer, the Ti/TiN multilayers have lower hardness and residual stress but higher toughness. The Ti/TiN multilayer with 6 sccm nitrogen flow rate has better wear resistance than the Ti/TiN multilayer with 2 sccm nitrogen flow rate but cracks during friction.
- (2) The TiN monolayer cannot provide wear protection for the magnesium alloy and fails after friction for 9 min. The Ti/TiN multilayers withstand the whole friction process, the minimum wear rate is 2.50×10^{-6} mm³/N. m, more than 3 orders of magnitude lower than that of the uncoated sample.
- (3) Coating structure and the deformation coordination between the coating and the magnesium alloy affect the wear resistance and wear mechanism of the coating. The TiN monolayer with columnar crystal has poor crack propagation resistance and poor deformation coordination with the magnesium alloy, which accelerates the failure of the coating.

(4) The excellent wear resistance of the Ti/TiN multilayers is attributed to the good crack propagation resistance and coordinated deformation ability with the magnesium alloy matrix. With increase of friction time, the multilayer film is worn layer by layer.

CRediT authorship contribution statement

Wenling Xie: Methodology, Validation, Data curation, Writing-Original draft.

Yiman Zhao: Formal analysis, Investigation. Bin Liao: Conceptualization, Resources. Shu Wang: Methodology, Supervision.

Sam Zhang: Conceptualization, Writing-Review & Editing.

Declaration of competing interest

The authors declare that they have no known competing financial interests or personal relationships that could have appeared to influence the work reported in this paper.

Acknowledgments

This work was supported by the Fundamental Research Funds for the Central Universities (SWU118105); and the Guangdong Province Key Area R&D Program (2019B090909002); and the National Natural Science Foundation Joint Fund Key Project (U1865206); and the Sichuan Provincial Key Lab of Process Equipment and Control (GK202011).

References

- [1] D. Khazeni, M. Saremi, R. Soltani, Development of HA-CNTs composite coating on AZ31 magnesium alloy by cathodic electrodeposition, part 1: microstructural and mechanical characterization, Ceram. Int. 45 (2019) 11174–11185.
- [2] A.S.H. Makhlouf, Y. Gajarla, in: A.S.H. Makhlouf, N. Abu-Thabit (Eds.), Chapter 8 -Advances in Smart Coatings for Magnesium Alloys and Their Applications in Industry, Elsevier Inc, 2020, pp. 245–261.
- [3] B.L. Mordike, T. Ebert, Magnesium: properties- applications- potential, Mater. Sci. Eng., A A302 (2001) 37–45.
- [4] C. Yang, H. Cai, S. Cui, J. Huang, J. Zhu, Z. Wu, Z. Ma, R.K.Y. Fu, L. Sheng, X. Tian, P.K. Chu, Z. Wu, A zinc-doped coating prepared on the magnesium alloy by plasma electrolytic oxidation for corrosion protection, Surf. Coat. Technol. 433 (2022), 128148.
- [5] C. Ma, M. Zhang, Y. Yuan, X. Jing, X. Bai, Tribological behavior of plasma electrolytic oxidation coatings on the surface of mg-8Li-1Al alloy, Tribol. Int. 47 (2012) 62–68.
- [6] X.-J. Cui, C.-M. Ning, G.-A. Zhang, L.-L. Shang, L.-P. Zhong, Y.-J. Zhang, Properties of polydimethylsiloxane hydrophobic modified duplex microarc oxidation/ diamond-like carbon coatings on AZ31B mg alloy, J. Magnesium Alloys 9 (2020) 1285–1296.
- [7] G. Wu, X. Zeng, S. Yao, X. Wang, Formation of a novel nanocrystalline coating on AZ31 magnesium alloy by bias sputtering, Mater. Lett. 61 (2007) 4019–4022.
- [8] X. Zeng, G. Wu, S. Yao, Formation by reactive magnetron sputtering of TiN coating on ti-implanted magnesium alloy, Mater. Lett. 60 (2006) 2252–2255.
- [9] X.J. Cui, C.M. Ning, L.L. Shang, G.A. Zhang, X.Q. Liu, Structure and anticorrosion, friction, and wear characteristics of pure diamond-like carbon (DLC), cr-DLC, and cr-H-DLC films on AZ91D mg alloy, J. Mater. Eng. Perform. 28 (2019) 1213–1225.
- [10] Z. Xie, Z. Luo, Y. Qin, C. Tian, T. Sheng, Y. Wang, Y. Luo, Improving anti-wear and anti-corrosion properties of AM60 magnesium alloy by ion implantation and Al/ AlN/CrAlN/CrN/MoS2 gradient duplex coating, Vacuum 101 (2014) 171–176.
- [11] Q. Miao, C.E. Cui, J.D. Pan, L.H. Duan, Y.P. Liu, Tribological behavior of magnesium alloy AZ91 coated with TiN/CrN by arc-glow plasma depositing, Chin. J. Aeronaut. 19 (2006) 266–270.
- [12] Q. Miao, C.E. Cui, J.D. Pan, P.Z. Zhang, Improving wear resistance of magnesium alloy AZ91D by TiN-CrN multilayer coating, Trans. Nonferrous Metals Soc. China 16 (2006) 1802–1805.
- [13] M. Hu, Y. Liu, The research of modulation period on photoelectric properties of Ti/ TiN multilayer films, Adv. Mater. Res. 126–128 (2010) 935–939.
- [14] J.M. Lackner, Industrially-scaled room-temperature pulsed laser deposition of ti-TiN multilayer coatings, J. Phys. Conf. Ser. 59 (2007) 16–21.
- [15] E. Kusano, M. Kitagawa, H. Nanto, A. Kinbara, Hardness enhancement by compositionally modulated structure of Ti/TiN multilayer films, J. Vac. Sci. Technol. A 16 (1998) 1272–1276.
- [16] J. Lackner, L. Major, M. Kot, Microscale interpretation of tribological phenomena in Ti/TiN soft-hard multilayer coatings on soft austenite steel substrates, Bull. Pol. Acad. Sci.: Tech. Sci. 59 (2011) 344–355.

- [17] R. Ali, M. Sebastiani, E. Bemporad, Influence of ti-TiN multilayer PVD-coatings design on residual stresses and adhesion, Mater. Des. 75 (2015) 47–56.
- [18] E. Bemporad, M. Sebastiani, C. Pecchio, S.D. Rossi, High thickness Ti/TiN multilayer thin coatings for wear resistant applications, Surf. Coat. Technol. 201 (2006) 2155–2165.
- [19] H. Holleck, V. Schier, Multilayer PVD coatings for wear protection, Surf. Coat. Technol. 76–77 (1995) 328–336.
- [20] C. Zhao, Y. Zhu, Z. Yuan, J. Li, Structure and tribocorrosion behavior of Ti/TiN multilayer coatings in simulated body fluid by arc ion plating, Surf. Coat. Technol. 403 (2020), 126399.
- [21] M. Hu, Y. Liu, Z.Q. Lai, Technological parameters and electrical properties of Ti/ TiN multilayer films prepared by magnetron sputtering, Mater. Sci. Forum 654–656 (2010) 1752–1755.
- [22] C. Liu, P.K. Chu, G. Lin, D. Yang, Effects of Ti/TiN multilayer on corrosion resistance of nickel-titanium orthodontic brackets in artificial saliva, Corros. Sci. 49 (2007) 3783–3796.
- [23] S.-S. Lin, K.-S. Zhou, M.-J. Dai, F. Hu, Q. Shi, H.-J. Hou, C.-B. Wei, F.-Q. Li, X. Tong, Effects of surface roughness of substrate on properties of Ti/TiN/Zr/ZrN multilayer coatings, Trans. Nonferrous Met. Soc. China 25 (2015) 451–456.
- [24] V.F. Gorban, A.O. Andreev, V.A. Stolbovoi, A.M. Myslyvchenko, A.D. Kostenko, Properties of metal-metal nitride vacuum-arc multilayer coatings, J. Superhard Mater. 42 (2020) 67–72.
- [25] A. Leyland, A. Matthews, Thick Ti/TiN multilayered coatings for abrasive and erosive wear resistance, Surf. Coat. Technol. 70 (1994) 19–25.
- [26] A. Kashyap, A.P. Harsha, H.C. Barshilia, V. Bonu, R.K. Singh, Study of tribological properties of multilayer Ti/TiN coating containing stress absorbing layers, J. Tribol. 142 (2020), 111401.
- [27] L.A.S. Ries, D.S. Azambuja, I.J.R. Baumvol, Corrosion resistance of steel coated with Ti/TiN multilayers, Surf. Coat. Technol. 89 (1997) 114–120.
- [28] J.F. Marco, A.C. Agudelo, J.R. Gancedo, D. Hanzel, Corrosion resistance of single TiN layers, Ti/TiN bilayers and Ti/TiN/Ti/TiN multilayers on iron under a salt fog spray (phohesion) test: an evaluation by XPS, Surf. Interface Anal. 27 (1999) 71–75.
- [29] S. Zhu, Y. Wu, Z. Li, L. Fang, A. Yin, J. Yan, F. Jiang, X. Meng, P. Chen, Z. Cai, Fretting wear behavior and photoelectron spectroscopy (XPS) analysis of a Ti/TiN multilayer film deposited on depleted uranium, Materials 11 (2018) 1538.
- [30] X. Cao, W. Xu, W. He, A method for evaluating the impact wear behavior of multilayer TiN/Ti coating, Coatings 10 (2020) 13201–13210.
- [31] H. Zhang, Z. Li, W. He, C. Ma, B. Liao, Damage mechanisms evolution of TiN/Ti multilayer films with different modulation periods in cyclic impact conditions, Appl. Surf. Sci. 540 (2021), 148366.
- [32] B. Coto, P. Hallander, L. Mendizabal, F. Pagano, L.J.W. Selegrd, Particle and Rain Erosion Mechanisms on Ti/TiN Multilayer PVD Coatings for Carbon Fibre Reinforced Polymer Substrates Protection 466-467, 2021.
- [33] J.-Y. Chen, G.-P. Yu, J.-H. Huang, Corrosion behavior and adhesion of ion-plated TiN films on AISI 304 steel, Mater. Chem. Phys. 65 (2000) 310–315.
- [34] G.C.A.M. Janssen, M.M. Abdalla, F.V. Keulen, B.R. Pujada, B.V. Venrooy, Celebrating the 100th anniversary of the stoney equation for film stress: developments from polycrystalline steel strips to single crystal silicon wafers, Thin Solid Films 517 (2009) 1858–1867.
- [35] H.N. Vatan, R. Ebrahimi-kahrizsangi, M. Kasiri-asgarani, Structural, tribological and electrochemical behavior of SiC nanocomposite oxide coatings fabricated by plasma electrolytic oxidation (PEO) on AZ31 magnesium alloy, J. Alloys Compd. 683 (2016) 241–255.
- [36] W. Xie, Y. Zhao, B. Liao, P. Pang, D. Wuu, S. Zhang, Al-AlN composite coatings on AZ31 magnesium alloy for surface hardening and corrosion resistance, Vacuum 188 (2021), 110146.
- [37] D. Zhang, Z. Qi, B. Wei, H. Shen, Z. Wang, Microstructure and corrosion behaviors of conductive Hf/HfN multilayer coatings on magnesium alloys, Ceram. Int. 44 (2018) 9958–9966.
- [38] B. Subramanian, R. Ananthakumar, V.S. Vidhya, M. Jayachandran, Influence of substrate temperature on the materials properties of reactive DC magnetron sputtered Ti/TiN multilayered thin films, Mater. Sci. Eng. B 176 (2011) 1–7.
- [39] W. Dai, G. Wu, A. Wang, Preparation, characterization and properties of crincorporated DLC films on magnesium alloy, Diam. Relat. Mater. 19 (2010) 1307–1315.
- [40] W. Yang, P. Ke, Y. Fang, H. Zheng, A. Wang, Microstructure and properties of duplex (Ti:N)-DLC/MAO coating on magnesium alloy, Appl. Surf. Sci. 270 (2013) 519–525.
- [41] M. Dong, X. Cui, G. Jin, H. Wang, L. Zhu, J. Liu, The mechanical and corrosion resistance properties of Ti/TiN multi-layer films produced by physical vapor deposition, Anti-Corros. Methods Mater. 62 (2015) 149–155.
- [42] M. Wen, C.Q. Hu, Q.N. Meng, Z.D. Zhao, T. An, Y.D. Su, W.X. Yu, W.T. Zheng, Effects of nitrogen flow rate on the preferred orientation and phase transition for niobium nitride films grown by direct current reactive magnetron sputtering, J. Phys. D. Appl. Phys. 42 (2009), 035304.
- [43] K. Shukla, R. Rane, J. Alphonsa, P. Maity, S. Mukherjee, Structural, mechanical and corrosion resistance properties of Ti/TiN bilayers deposited by magnetron sputtering on AISI 316L, Surf. Coat. Technol. 324 (2017) 167–174.
- [44] A. Vladescu, C. Cotrut, M. Balaceanu, V. Braic, A. Kiss, M. Braic, S. Zamfir, Ti/TiN multilayer coatings for orthopedic implants, Rom. J. Phys. 49 (2004) 949–954.
- [45] M. Bai, K. Kato, N. Umehara, Y. Miyake, Nanoindentation and FEM study of the effect of internal stress on micro/nano mechanical property of thin CNx films, Thin Solid Films 377–378 (2000) 138–147.

- [46] A. Mubarak, E.B. Hamzah, The effect of nitrogen gas flow rate on the properties of TiN-coated high-speed steel (Hss) using cathodic arc evaporation physical vapor deposition (PVD) technique, Surf. Rev. Lett. 12 (2005) 631–643.
- [47] Q. Zhang, Y.X. Leng, F. Qi, T. Tao, N. Huang, Mechanical and corrosive behavior of Ti/TiN multilayer films with different modulation periods, Nucl. Inst. Methods Phys. Res. B 257 (2007) 411–415.
- [48] J.M. González-Carmona, J.D. Triviño, Á. Gómez-Ovalle, C. Ortega, J.M. Alvarado-Orozco, H. Sánchez-Sthepa, A. Avila, Wear mechanisms identification using kelvin probe force microscopy in TiN, ZrN and TiN/ZrN hard ceramic multilayers coatings, Ceram. Int. 46 (2020) 24592–24604.
- [49] A. Leyland, A. Matthews, On the significance of the H/E ratio in wear control: a nanocomposite coating approach to optimised tribological behaviour, Wear 246 (2000) 1–11.
- [50] T. Liu, C. Dong, S. Wu, K. Tang, J. Wang, J. Jia, TiN, TiN gradient and Ti/TiN multi-layer protective coatings on uranium, Surf. Coat. Technol. 201 (2007) 6737–6741.
- [51] L.S. Wen, R.F. Huang, L.P. Guo, J. Gong, T.Y. Wei, Y.Z. Chuang, Microstructure and mechanical properties of metal/ceramic Ti/TiN multilayers, J. Magn. Magn. Mater. 126 (1993) 200–202.

- [52] Y. Wei, X. Zong, Z. Jiang, X. Tian, Characterization and mechanical properties of TiN/TiAlN multilayer coatings with different modulation periods, Int. J. Adv. Manuf. Technol. 96 (2018) 1677–1683.
- [53] W. Yang, G. Ayoub, I. Salehinia, B. Mansoor, H. Zbib, Deformation mechanisms in Ti/TiN multilayer under compressive loading, Acta Mater. 122 (2017) 99–108.
- [54] L. Major, J. Morgiel, TEM analysis of wear of Ti/TiN multi-layer coating in ball-ondisc test, Key Eng. Mater. 409 (2009) 123–127.
- [55] C.L. Jiang, H.L. Zhu, K.S. Shin, Y.B. Tang, Influence of titanium interlayer thickness distribution on mechanical properties of Ti/TiN multilayer coatings, Thin Solid Films 632 (2017) 97–105.
- [56] K.J. Ma, A. Bloyce, T. Bell, Examination of mechanical properties and failure mechanisms of TiN and ti-TiN multilayer coatings, Surf. Coat. Technol. 76 (1995) 297–302.
- [57] S. Wang, Analysis on bearing capacity of steel frame structure and coating, Hoisting Transp. Mach. China (2013) 55–59.
- [58] M.Y. He, A.G. Evans, J.W. Hutchinson, Structures, crack deflection at an interface between dissimilar elastic materials: role of residual stresses, Int. J. Solids Struct. 31 (1994) 3443–3455.